nuclear localization is important in establishing transcriptionally silent chromatin. □

Methods

Strains and plasmids. Strains YSB35, YSB2, YSB41 and YSB2 were used to measure targeted silencing as described[10]. All five membrane proteins were cloned in-frame into the overexpression vector pMA424 (ref. 23) to create G_{BD} hybrids. The entire coding sequence was used for YIP1 (pEDA73) and MNN10 (pEDA96). The YIP3 hybrid encompassed amino acids 39–182 (pEDA85); the YIF1 hybrid, amino acids 55–314 (pEDA76); and the STT3 hybrid, amino acids 45–720 (pEDA93). G_{BD}–MNN10 (pEDA109) was constructed by digesting pEDA96 with *Eco*RI and *Sal*I and subcloning the MNN10 fragment into pGBT9C. To make MNN10–G_{BD}, a PCR fragment with the MNN10 coding region was cloned into the *Bam*HI site of the C-terminal G_{BD} fusion vector D134 (gift from R. Brazas). The SIR3 and SIR4 overexpression plasmids were pJR104 and pHR643, respectively (from J. Rine's laboratory).

Indirect immunofluorescence and western blot analysis. For immunofluorescence, cells were grown to mid-log phase, fixed with formaldehyde and prepared as described[24]. The primary antibody used was one directed against G_{BD} (Upstate Biotechnology). For western blots, strain YSB35 transformants were grown to an absorbance at 600 nm of 1.0 and lysed by vortexing with glass beads. Western blotting was done as described[25] using the same anti-G_{BD} primary antibody to detect G_{BD} hybrids.

Received 23 March; accepted 16 June 1998.

1. Hecht, A., Laroche, T., Strahl-Bolsinger, S., Gasser, S. M. & Grunstein, M. Histone H3 and H4 N-termini interact with the silent information regulators Sir3 and Sir4: A model for the formation of heterochromatin in yeast. *Cell* **80,** 583–592 (1995).
2. Triolo, T. & Sternglanz, R. Role of interactions between the origin recognition complex and SIR1 in transcriptional silencing. *Nature* **381,** 251–253 (1996).
3. Hecht, A., Strahl-Bolsinger, S. & Grunstein, M. Spreading of transcriptional repression by SIR3 from telomeric heterochromatin. *Nature* **383,** 92–96 (1996).
4. Strahl-Bolsinger, S., Hecht, A., Luo, K. & Grunstein, M. SIR2 and SIR4 interactions in core and extended telomeric heterochromatin in yeast. *Genes Dev.* **11,** 83–93 (1997).
5. Gotta, M. *et al.* The clustering of telomeres and colocalization with Rap1, Sir3, and Sir4 proteins in wild-type *Saccharomyces cerevisiae*. *J. Cell Biol.* **134,** 1349–1363 (1996).
6. Hiraoka, Y., Agard, D. A. & Sedat, J. W. Temporal and spatial coordination of chromosome movement, spindle formation, and nuclear envelope breakdown during prometaphase in *Drosophila melanogaster* embryos. *J. Cell. Biol.* **11,** 2815–2828 (1990).
7. Funabiki, H., Hagan, I., Usawa, S. & Yanagida, M. Cell cycle dependent specific positioning and clustering of centromeres and telomeres in fission yeast. *J. Cell Biol.* **121,** 961–976 (1993).
8. Marshall, W. F., Dernburg, A. F., Harmon, B., Agard, D. A. & Sedat, J. W. Specific interactions of chromatin with the nuclear envelope: Positional determination within the nucleus in *Drosophila melanogaster*. *Mol. Biol. Cell* **7,** 825–842 (1996).
9. Brand, A. H., Breeden, L., Abraham, J., Sternglanz, R. & Nasmyth, K. Characterization of a "silencer" in yeast: A DNA sequence with properties opposite to those of a transcriptional enhancer. *Cell* **41,** 41–48 (1985).
10. Chien, C.-T., Buck, S., Sternglanz, R. & Shore, D. Targeting of SIR1 protein establishes transcriptional silencing at *HM* loci and telomeres in yeast. *Cell* **75,** 531–541 (1993).
11. Buck, S. W. & Shore, D. Action of a RAP1 carboxy-terminal silencing domain reveals an underlying competition between *HMR* and telomeres in yeast. *Genes Dev.* **9,** 370–384 (1995).
12. Marcand, S., Buck, S. W., Moretti, P., Gilson, E. & Shore, D. Silencing of genes at nontelomeric sites in yeast is controlled by sequestration of silencing factors at telomeres by Rap1 protein. *Genes Dev.* **10,** 1297–1309 (1996).
13. Munro, S. Sequences within and adjacent to the transmembrane segment of the α-2,6-sialyltransferase specify Golgi retention. *EMBO J.* **10,** 3577–3588 (1991).
14. Machamer, C. E. *et al.* Retention of a *cis* Golgi protein requires polar residues on one face of a predicted α-helix in the transmembrane domain. *Mol. Biol. Cell* **4,** 695–704 (1993).
15. Dean, N. & Poster, J. Molecular and phenotypic analysis of the *S. cerevisiae MNN10* gene identifies a family of related glycosyltransferases. *Glycobiology* **6,** 73–81 (1996).
16. Zufferey, R. *et al.* STT3, a highly conserved protein required for yeast oligosaccharyl transferase activity *in vivo*. *EMBO J.* **14,** 4949–4960 (1995).
17. Karaoglu, D., Kelleher, D. J. & Gilmore, R. The highly conserved Stt3 protein is a subunit of the yeast oligosaccharyltransferase and forms a subcomplex with Ost3p and Ost4p. *J. Biol. Chem.* **272,** 32513–32520 (1997).
18. Khosravi-Far, R. *et al.* Isoprenoid modifcation of rab proteins terminating in CC or CXC motifs. *Proc. Natl Acad. Sci. USA* **88,** 6264–6268 (1991).
19. Kinsella, B. T. & Maltese, W. A. *rab* GTP-binding proteins with three different carboxyl-terminal cysteine motifs are modified *in vivo* by 20-carbon isoprenoids. *J. Biol. Chem.* **267,** 3940–3945 (1992).
20. Maillet, L. *et al.* Evidence for silencing compartments within the yeast nucleus: a role for telomere proximity and Sir protein concentration in silencer-mediated repression. *Genes Dev.* **10,** 1796–1811 (1996).
21. Stone, E. M., Swanson, M. J., Romeo, A. M., Hicks, J. B. & Sternglanz, R. The *SIR1* gene of *Saccharomyces cerevisiae* and its role as an extragenic suppressor of several mating-defective mutants. *Mol. Cell. Biol.* **11,** 2253–2262 (1991).
22. Renauld, H. *et al.* Silent domains are assembled continuously from the telomere and are defined by promoter distance and strength, and *SIR3* dosage. *Genes Dev.* **7,** 1133–1145 (1993).
23. Ma, J. & Ptashne, M. A new class of yeast transcriptional activators. *Cell* **51,** 113–119 (1987).
24. Pringle, J. R., Adams, A. E. M., Drubin, G. & Haarer, B. K. Guide to yeast genetics and molecular biology. *Meth. Enzymol.* **194,** 565–602 (1991).
25. Harlow, E. & Lane, D. *Antibodies: A Laboratory Manual* (CSHL Press, Cold Spring Harbor, NY, 1988).
26. Kaiser, C. A. & Schekman, R. Distinct sets of *SEC* genes govern transport vesicle formation and fusion early in the secretory pathway. *Cell* **61,** 723–733 (1990).

Supplementary information is available on *Nature*'s World-Wide Web site (http://www.nature.com) or as paper copy from the London editorial office of *Nature*.

Acknowledgements. We thank D. Gallwitz for communicating unpublished results; N. Dean, H. Park, S. Marcand, D. Shore and R. Brazas for plasmids and strains; and N. Dean, A. Mook and C. Dingwall for advice and comments. This work was supported by a grant from the NIH.

Correspondence and requests for materials should be addressed to R.S. (e-mail:rolf@life.bio.sunysb.edu).

Crystal structure of a small heat-shock protein

Kyeong Kyu Kim, Rosalind Kim & Sung-Hou Kim

Physical Biosciences Division of the Lawrence Berkeley National Laboratory and the Department of Chemistry, University of California at Berkeley, 220 Melvin Calvin Laboratory, Berkeley, California 94720-5230, USA

The principal heat-shock proteins that have chaperone activity (that is, they protect newly made proteins from misfolding) belong to five conserved classes: HSP100, HSP90, HSP70, HSP60 and the small heat-shock proteins (sHSPs). The sHSPs can form large multimeric structures and have a wide range of cellular functions, including endowing cells with thermotolerance *in vivo*[1,2] and being able to act as molecular chaperones *in vitro*[3–8]; sHSPs do this by forming stable complexes with folding intermediates of their protein substrates[9,10]. However, there is little information available about these structures or the mechanism by which substrates are protected from thermal denaturation by sHSPs. Here we report the crystal structure of a small heat-shock protein from *Methanococcus jannaschii*, a hyperthermophilic archaeon. The monomeric folding unit is a composite β-sandwich in which one of the β-strands comes from a neighbouring molecule. Twenty-four monomers form a hollow spherical complex of octahedral symmetry, with eight trigonal and six square 'windows'. The sphere has an outer diameter of 120 Å and an inner diameter of 65 Å.

The sHSPs are abundant and ubiquitous in nature; they range in size from 12K to 42K and are found as large complexes of 200K–800K. The sHSPs share a sequence of about 100 residues which is homologous to α-crystallin from the vertebrate eye lens, and is called the α-crystallin domain or small-heat-shock-protein domain. The sHSP from *M. jannaschii* (MjHSP16.5, relative molecular mass 16.5K)[11] also contains an α-crystallin domain composed of 90 residues (Fig. 1, residues 46 to 135). The domain has 20.7% sequence identity with human αA-crystallin and 31.4% identity with rice HSP16.9 (refs 3, 12). The protein forms homogeneous oligomers and has molecular chaperone activity[13]. We have determined the crystal structure of MjHSP16.5 from *M. jannaschii* at 2.9 Å resolution by using single isomorphous replacement and non-crystallographic symmetry (NCS) averaging (Table 1 and Fig. 2).

MjHSP16.5 is a hollow spherical complex composed of 24 subunits generated by a three-fold crystallographic symmetry operation of an asymmetric unit containing eight subunits (Fig. 3a). These eight subunits, in turn, are related by three kinds of NCS: four two-fold, one three-fold, and one four-fold symmetries. Therefore, 24 subunits in the complex are related by an octahedral symmetry, with a total of twelve two-fold, three three-fold, and three four-fold NCS axes, and one three-fold crystallographic symmetry axis[11] (Fig. 3a). The outer diameter of the sphere is ~120 Å, and the inner diameter is ~65 Å (Fig. 3b). The inside of the sphere is hollow and no remarkable electron density is found at the current resolution. There are eight triangular and six square windows on the surface of the sphere.

Each folding unit is composed of nine β-strands in two sheets, two short 3_{10}-helices, and one short β-strand (Fig. 4a). One of the β-strands comes from a neighbouring subunit. The amino-terminal 32 residues are highly disordered, but from residue 33 onwards, including the entire α-crystallin domain (residues 46–135) and

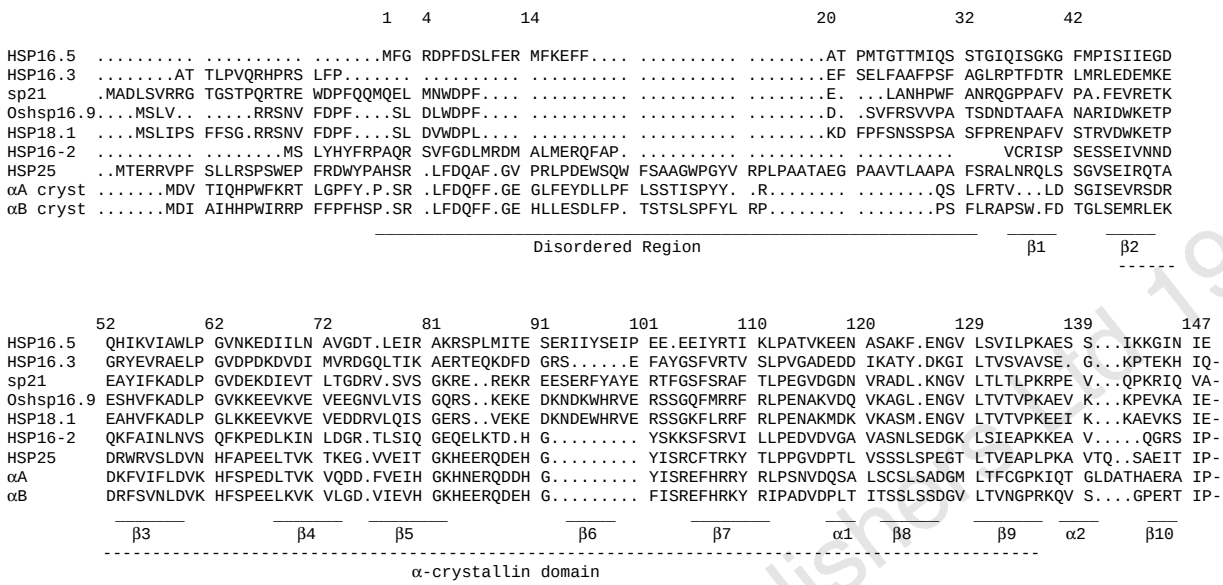

Figure 1 Sequence alignment of HSP16.5 with other small heat-shock proteins and α-crystallins. The alignment was performed with 'pileup' in the GCG program package[27]. The sequences aligned are from *M. jannaschii* HSP16.5, *Mycobacterium tuberculosis* HSP16.3, *Stigmatella aurantiaca* sp21, rice Oshsp16.9, pea HSP18.1, *C. elegans* HSP16-2, murine HSP25, bovine αA-crystallin, and bovine αB-crystallin. The alignment is made only until the last amino acid of HSP16.5. The secondary structure of HSP16.5 was assigned using PROCHECK[26], and the β-strands are labelled β1–β10.

the carboxy-terminal extension, they are well ordered. The overall structure of the folding unit has dimensions of 25 Å × 28 Å × 75 Å. The longest dimension is parallel to the length of the β-strands. Figure 1 shows the secondary structural elements of MjHSP16.5 aligned with homologous sHSPs. Two β-sheets are packed as parallel layers: β1, 7, 5 and 4 of one subunit in one β-sheet and β2, 3, 9 and 8 of the same subunit, and β6 of a neighbouring subunit in the other β-sheet. In addition, there are two short 3_{10}-helices (α1 and α2) and one short β-strand, β10. The folding pattern of the monomer is similar to a domain of the immunoglobulin Fc fragment, although there is no sequence similarity between them.

Each subunit in the MjHSP16.5 complex makes extensive contacts with other subunits in the complex. There are three different subunit–subunit contacts: the contacts related by the two-, three-, and four-fold NCSs (Figs 4b–d and Table 2). The most extensive subunit intersubunit contacts are found around the two-fold axis: the backbone atoms of the β2-strand in one subunit and the β6-strand in the other subunit (in a two-fold related dimer) form hydrogen bonds to make an intersubunit composite β-sheet. There are also extensive hydrophobic contacts and ionic interactions as well as interbackbone hydrogen bonds that stabilize the two subunits related by two-fold symmetry (Fig 4b, e and Table 2). The putative substrate-binding region of the α-crystallin domain of HSP18.1 which binds bis-ANS (ref. 10) is depicted in MjHSP16.5 (Fig. 4b) on the basis of the sequence alignment in Fig. 1 (loop between β3 and β4). In this loop, which is located outside the sphere, the conserved hydrophobic residues are involved in dimer interaction. Around the four-fold symmetry axis, four subunits make contact by hydrogen bonds, ionic, and hydrophobic interactions (Fig. 4c, e and Table 2). The C-terminal region (residues 142 to 147) of one subunit reaches out and interacts with β4 and β8 of a neighbouring subunit by hydrophobic interaction and backbone hydrogen bonding. One residue at the C terminus (Lys 141) is also involved in ionic interactions in this contact (Fig. 4e). Interactions among the subunits around the three-fold axis are the least extensive: one ionic interaction per subunit pair stabilizes two adjacent subunits at each corner of the triangular window (Fig. 4d, e and Table 2). Forty-one per cent of the solvent-accessible surface in each MjHSP16.5 monomer is buried at the intersubunit contacts (3,247 Å^2 out of 7,911 Å^2). Of these, 48% of the contact surfaces contribute to dimer formation, 42% to tetramer formation, and only 10% to trimer formation. Of the dimer contacts, 66% are due to nonpolar interactions, whereas only 31% are nonpolar interactions in the tetramer. Combined with the composite nature of the folding unit described earlier, this suggests that the dimer may be the building block of the sphere.

The interior of the MjHSP16.5 spherical structure appears to be empty at the current resolution. The inside volume of the sphere is about 140,000 Å^3, which is about 56% of the GroEL cylinder[14]. Thr 33, the first ordered residue in the subunit, is located inside the sphere and near the small square window around each four-fold symmetry axis. This suggests that the disordered N-terminal residues are inside the sphere, which is in agreement with the observation that the N terminus of HSP16-2 from *Caenorhabditis elegans* was found to be buried in the complex[15]. Interestingly, 49% of the solvent-accessible surfaces in the interior of the sphere are composed of nonpolar residues, in contrast to 22% on the outside surface, which is reminiscent of the GroEL structure[14]. This implies that the inside surface of the sphere is much more hydrophobic than the outside surface, although a part of this may be due to the areas

Table 1 Crystallographic data

Data collection and phasing statistics Crystal	Native (CuKα)	Native (NSLS)	Se-Met
Resolution (Å)	30.0–3.2	30.0–2.9	30.0–3.2
Completeness	98.2%	99.7%	99.9%
R_{sym}	0.071	0.037	0.069
R_{merge}			0.11
R_{cullis} (%)*			0.78
Phasing power†			1.0
Figure of merit (20.0–3.2)			0.258
Refinement statistics			
Resolution		15.0–2.9 Å	
NCS-related monomers/asymmetric unit		8	
Unique reflections ($F > 2\sigma$)		22,008	
Completeness ($F > 2\sigma$)		80.6% (8.96)‡	
R factor§		0.216 (0.251)‡	
Bond-length deviation from ideality		0.012 Å	
Bond-length deviation from ideality		1.505 deg	

* R_{cullis} is the r.m.s. lack-of-error divided by the isomorphous difference.
† Phasing power is the mean F_h divided by the r.m.s. lack-of-error.
‡ Values for the test data aside to calculate the free R factor.
§ R factor calculation was made from the data with 2σ cutoff.

Table 2 Intersubunit contacts in HSP16.5

Three-fold	
A	
B	Arg 93–Glu 78
C	
Four-fold	
A	142O–72N, 142N–72O, 144N–70O, 145O–122N, 147N–122O
B	Asp 51–Arg 80, Lys 141–Glu 78
C	Ile 144–Leu 70, Ala 72, Leu 77, Ala 120, Ala 122, Val 131, Leu 133*; Ile 146–Ile 68, Leu 70, Ala 122, Phe 124, Leu 129
Two-fold	
A.	45O–98N, 47N–96O, 47O–95N, 47O–96N, 49N–93O, 49O–93N, 126O–62N
B.	Glu 92–His 53, Glu 92–Lys 55, Glu 49–Arg 93, Asp 51–Arg 93
C.	Phe 42–Phe 42, Trp 59, Pro 44; Pro 61–Trp 59, Pro 61, Gly 127; Gly 62–Phe 42, Val 128; Ile 86–Ile 48, Ile 57; Ile 88–Ile 48; Ile 94–Ile 48; Ile 95–Ile 35, Ile 47, Pro 112; Tyr 96–Ile 35, Ile 37, Ile 45, Ile 47; Ile 99–Ile 57, Trp 59; Pro 100–Trp 59

A, Backbone hydrogen bond.
B, Side-chain ionic interaction or hydrogen bond.
C, Hydrophobic interaction.
* Ile 144 in one monomer interacts with the listed residues in the neighbouring monomer.

covered by the disordered N-terminal residues.

There are eight triangular windows and six square windows with the edges of the window frames being 30 Å and 17 Å, respectively (calculated with the side-chain atoms beyond Cβ deleted), on the surface of the hollow sphere of MjHSP16.5. Several negatively charged residues between β5 and β7 (Glu 90, Glu 101, Glu 103, and Glu 104) are located around the triangular windows. There are some charged residues (Asp 75, Lys 110, Glu 117, and Glu 118) around the square windows. These features are similar to those of the GroES structure, where there are two Glu residues around the orifice in the centre of the roof of the GroEL dome[16]. The size of the windows is large enough to allow small molecules such as enzyme substrates and products to diffuse in and out of the sphere. The triangular windows may be wide enough to allow even extended peptide chains to thread through them.

As the α-crystallin domain of MjHSP16.5 has a well ordered folded structure and is involved in subunit contacts, oligomeric complexes are probably due to the α-crystallin domain. The hydrophobic residues in the α-crystallin domain that are involved in maintaining the tertiary structure of the folding unit are relatively well conserved among all species (Fig. 1). This is consistent with the finding that the predicted secondary structures and hydrophobic profiles of the α-crystallin domains of the sHSP family (animal, plant and bacteria) are almost identical to those of MjHSP16.5 (ref. 17). However, some of the residues involved in subunit contacts are not conserved among all sHSPs (Fig. 1 and Table 2), suggesting that the size and the symmetry of oligomers may vary among different sHSPs although the unique fold of the sHSP monomer is conserved.

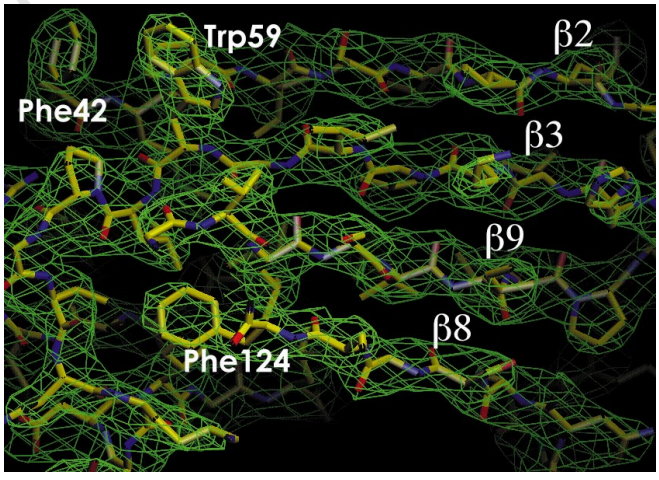

Figure 2 Representative region of the experimental electron density map contoured at 1.2σ. One β-sheet region and three hydrophobic residues are labelled.

Among the diverse physiological functions of sHSPs, their *in vitro* chaperone activity appears to be common to most sHSPs. The assumption that the highly conserved α-crystallin domain may be important for chaperone activity is contradicted by the observation that *Escherichia coli* expressing a rice protein deletion mutant, Oshsp16.9, fused to glutathione-*S*-transferase, where the C-terminal two-thirds of the α-crystallin domain is missing, is protected from heat shock[18]. Another related observation is that mutations within the phenylalanine-rich region of αB-crystallin, located N-terminal to the α-crystallin domain, abolish chaperone activity *in vitro* without altering the size of their oligomeric complex[19]. The N-terminal regions seem to be necessary for oligomerization because the minimal α-crystallin domain alone fails to form oligomers and has no chaperone activity *in vitro*[20,21]. Taken together, these observations seem to suggest that, although the α-crystallin domain is important in oligomeric-complex formation, the N-terminal residues before the α-crystallin domain are necessary not only for complex formation but also for chaperone activity.

There are many possible mechanisms to explain sHSPs' ability to protect other proteins from denaturation. One is that during the process of *in vivo* assembly of the hollow spheres, certain proteins or RNAs critical for the cells' survival under stress may get trapped in or on the outer surface of the spheres. Another is that the oligomeric

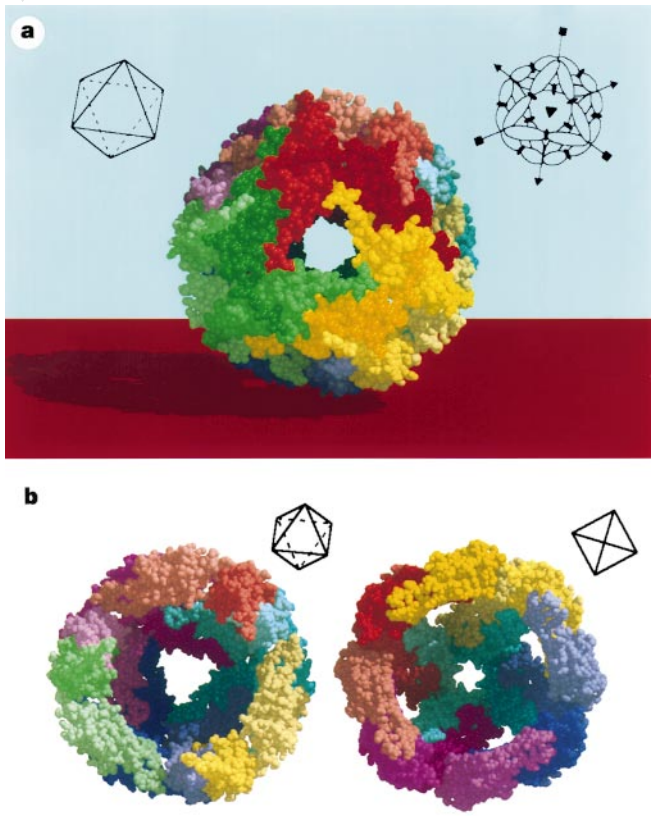

Figure 3 Overall structure of sHSP. **a**, A space-filling model of the hollow sphere viewed along the crystallographic three-fold axis. Each HSP16.5 tetramer is represented in one colour with different shadings. Top right, schematic of the 24 subunits, drawn as ovals, and their symmetry elements; top left, octahedral symmetry of sHSP. The holes in the shadow of the sphere are generated by the triangular and square windows. **b**, The interior of the sphere is viewed along the three-fold axis (left) and the four-fold axis (right). The front one-third of each sphere is cut off to reveal the inside of the hollow sphere. Colour code as in **a**. An octahedron oriented in the same way as the corresponding sHSP is shown at the top.

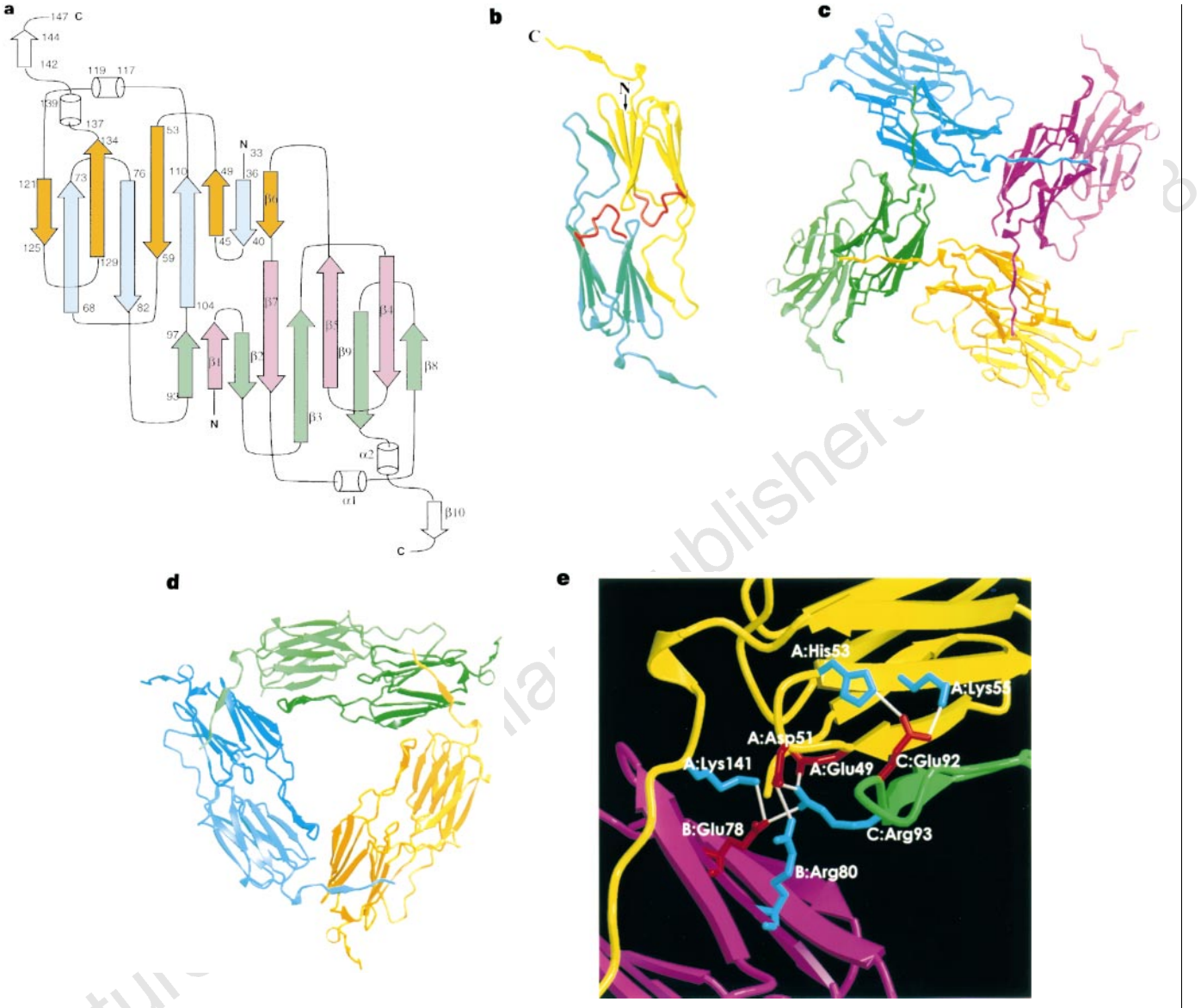

Figure 4 Subunit interaction of sHSP. **a**, Topology of the secondary structure of a MjHSP16.5 dimer. The first and last residue numbers for each secondary-structural element are indicated in the top (left) monomer; the secondary-structural elements are labelled in the monomer at the bottom (right). The first β-sheet of the top monomer is in blue and the second β-sheet is in yellow, but β6 (also yellow) is from the adjacent subunit. The first and second β-sheets of the bottom monomer are also shown in different colours (green and pink, respectively). **b**, Ribbon diagram of an HSP16.5 dimer viewed along the non-crystallographic two-fold symmetry axis. The N and C termini are indicated. The bis-ANS binding sites in the α-crystallin domain of HSP18.1 (ref. 10) are shown in red. **c**, Four dimers related by a non-crystallographic four-fold symmetry. **d**, Three dimers related by a non-crystallographic three-fold symmetry. **e**, Several residues that are involved in ionic interaction in subunit contacts (Table 2) are shown. Subunits A (yellow) and B (magenta) are related by four-fold symmetry, B and C (green) by three-fold symmetry, and A and C by two-fold symmetry. Basic residues are coloured blue and acidic residues are coloured red. Possible ionic interactions are represented as white lines.

form of sHSP is not necessary for chaperone or other stress-related activity, but is a storage state for sHSPs from which they can be disassembled quickly in response to the recurrence of external stress. □

Methods

Crystallization and data collection. MjHSP16.5 was purified and crystallized as described[11]. Selenomethionine-substituted protein was crystallized under the same conditions. X-ray data of the native and selenomethionine-substrated crystals were collected at 3.2 Å resolution on a Rigaku R-Axis IIC imaging plate system. Another native data set was collected at 2.9 Å resolution at the beamline X12C at the National Synchrotron Light Source, Brookhaven (NSLS). The native and selenomethionine derivative data were processed and integrated by DENZO and scaled by SCALEPACK[22]. There are eight subunits in an asymmetric unit of the unit cell in the *R*3 space group with a V_m of 2.2 Å^3 dalton^{-1}.

Structure determination and refinement. The first selenium site was found in the difference Patterson map. The other seven selenium sites were found in the difference Fourier map by using the phase calculated from the first selenium site at 3.2 Å. Only eight out of 40 selenomethionines in an asymmetric unit were found. The initial model was built on the map calculated from the eight selenomethionine sites and modified by solvent flattening with a solvent content of 45%. Six NCS operators were found from the initial model: four two-fold, one three-fold, and one four-fold rotations. The phases were improved further by averaging over eight NCS-related subunits in an asymmetric unit using the program DM[23]. At this stage, the electron density showed a single polypeptide chain per monomer without any disconnectivity. Amino acids were assigned from residues 33 to 147 using program O[24]. The first 32 amino acids were unassignable because of disorder. The other seven subunits were generated from the first subunit model by the NCS operators.

Several cycles of rigid body refinement, positional refinement, and simulated

annealing with tight non-crystallographic restraints in X-plor[25] were performed at 3.2 Å resolution. The refinements were continued by using the native data at 2.9 Å resolution collected at the NSLS and resulted in an *R* value of 21.6% and a free *R* value of 25.1% with the bulk solvent correction and B-factor refinement. The refined model included eight subunits, each containing 116 residues from amino acids 33 to 147. The root-mean-squares deviation for all atoms among the eight subunits in an asymmetric unit is 0.041 Å. Most (85.2%) of the non-glycine amino acids were in the most favourable regions, and the remaining 14.8% were in the allowed region in the Ramachandran plot drawn by PROCHECK[26].

Received 29 April; accepted 9 June 1998.

1. Schirmer, E. C., Lindquist, S. & Vierling, E. An *Arabidopsis* heat shock protein complements a thermotolerance defect in yeast. *Plant Cell* **6,** 1899–1909 (1994).
2. van den IJssel, P. R., Overkamp, P., Knauf, U., Gaestel, M. & de Jong, W. W. Alpha A-crystallin confers cellular thermoresistance. *FEBS Lett.* **355,** 54–56 (1994).
3. Horwitz, J. Alpha-crystallin can function as a molecular chaperone. *Proc. Natl Acad. Sci. USA* **89,** 10449–10453 (1992).
4. Jacob, U., Gaestel, M., Engel, K. & Buchner, J. Small heat shock proteins are molecular chaperones. *J. Biol. Chem.* **268,** 1517–1520 (1993).
5. Merck, K. B. *et al*. Structural and functional similarities of bovine alpha-crystallin and mouse small heat-shock protein. A family of chaperones. *J. Biol. Chem.* **268,** 1046–1052 (1993).
6. Lee, G. J., Pokala, N. & Vierling, E. Structure and *in vitro* molecular chaperone activity of cytosolic small heat shock proteins from pea. *J. Biol. Chem.* **270,** 10432–10438 (1995).
7. Chang, Z. *et al*. *Mycobacterium tuberculosis* 16-kDa antigen (Hsp16.3) functions as an oligomeric structure *in vitro* to suppress thermal aggregation. *J. Biol. Chem.* **271,** 7218–7223 (1996).
8. Jaenicke, R. & Creighton, T. E. Junior chaperones. *Curr. Biol.* **3,** 234–235 (1993).
9. Ehrnsperger, M., Graber, S., Gaestel, M. & Buchner, J. Binding of non-native protein to Hsp25 during heat shock creates a reservoir of folding intermediates for reactivation. *EMBO J.* **16,** 221–229 (1997).
10. Lee, G. J., Roseman, A. M., Saibil, H. R. & Vierling, E. A small heat shock protein stably binds heat-denatured model substrates and can maintain a substrate in a folding-competent state. *EMBO J.* **16,** 659–671 (1997).
11. Kim, K. K., Yokota, H., Kim, S.-H. Purification, crystallization and preliminary X-ray crystallographic analysis of small heat shock protein homolog from *Methanococcus jannaschii*. *J. Struct. Biol.* **121,** 76–80 (1998).
12. Tseng, T. S. *et al*. Two rice (Oryza sativa) full-length cDNA clones encoding low-molecular-weight heat-shock proteins. *Plant Mol. Biol.* **18,** 963–965 (1992).
13. Kim, R., Kim, K. K., Yokota, H. & Kim, S.-H. Small heat shock protein of *Methanococcus jannaschii*, a hyperthermophile. *Proc. Natl Acad. Sci. USA* (in press).
14. Braig, K. *et al*. The crystal structure of the bacterial chaperonin GroEL at 2.8 Å. *Nature* **371,** 578–586 (1994).
15. Leroux, M., Melki, R., Gordon, B., Batelier, G. & Candido, E. P. M. Structure–function studies on small heat shock protein oligometric assembly and interaction with unfolded polypeptides. *J. Biol. Chem.* **272,** 24646–24656 (1997).
16. Hunt, J. F., Weaver, A. J., Landry, S. J., Gierasch, L. & Deisenhofer, J. The crystal structure of the GroES co-chaperonin at 2.8 Å resolution. *Nature* **379,** 37–45 (1996).
17. Caspers, G.-J., Leunissen, J. A. M. & de Jong, W. W. The expanding small heat-shock protein family, and structural predictions of the conserved "α-crystallin domain". *Mol. Evol.* **40,** 238–248 (1995).
18. Yeh, C. H. *et al*. Expression of a gene encoding a 16.9-kDa heat-shock protein, Oshsp16.9, in *Escherichia coli* enhances thermotolerance. *Proc. Natl Acad. Sci. USA* **94,** 10967–10972 (1997).
19. Plater, M. L., Goode, D. & Crabbe, M. J. C. Effects of site-directed mutations on the chaperone-like activity of αB-crystallin. *J. Biol. Chem.* **271,** 28558–28566 (1996).
20. Merck, K. B. *et al*. Comparison of the homologous carboxy-terminal domain and tail of alpha-crystallin and small heat shock protein. *Mol. Biol. Rep.* **18,** 209–215 (1993).
21. Leroux, M., Ma, B. J., Batelier, G., Melki, R. & Candido, E. P. M. Unique structural features of a novel class of small heat shock proteins. *J. Biol. Chem.* **272,** 12847–12853 (1997).
22. Otwinowski, Z. in *Data Collection and Processing* (eds Sawyer, L., Isaacs, N. & Bailey, S.) 56–62 (SERC Daresbury Laboratory, Warrington, UK, 1993).
23. Cowtain, K. D. & Main, P. Improvement of macromolecular electron-density maps by the simultaneous application of real and reciprocal space constraints. *Acta Crystallogr. D* **49,** 148–157, 1993.
24. Jones, T. A., Zou, J.-Y., Cowan, S. W. & Kjeldgaard, M. Improved methods for binding protein models in electron density maps and the location of errors in these models. *Acta Crystallogr. A* **47,** 110–119 (1991).
25. Brünger, A. T. *X-PLOR version 3.1* (Yale Univ. Press, New Haven, CT, 1993).
26. Laskowski, R. A., MacArthur, M. W., Moss, D. S. & Thronton, J. M. *J. Appl. Crystallogr.* **26,** 283–291 (1993).
27. Genetics Computer Group *Program manual for the GCG package, version 7* (GCG, Madison, WI, 1991).

Acknowledgements. We thank D. King for doing the electrospray mass spectrometry; H. Yokota for help with protein preparation, D. Boisvert for critical discussion of the manuscript, and R. Sweet at the NSLS for data collection. This work was funded by the US Department of Energy (R.K. and S.-H.K.).

Correspondence and requests for materials should be addressed to S.-H.K. (e-mail: SHKIM@LBL.GOV). The identity code of the coordinates and structure factors are 1SHS and R1SHSSF, respectively, in the Brookhaven Protein Data Bank.